This is an open access article published under an ACS AuthorChoice License, which permits copying and redistribution of the article or any adaptations for non-commercial purposes.

ACS OMEGA

Article

Cite This: ACS Omega 2019, 4, 14875−14885

http://pubs.acs.org/journal/acsodf

Development of Azo-Based Turn-On Chemical Array System for Hydrazine Detection with Fluorescence Pattern Analysis

Min Chul Shin,[†,⊥] Youngjun Lee,[‡,∥,⊥] Seung Bum Park,[*,‡,§] and Eunha Kim[*,†]

[†]Department of Molecular Science and Technology, Ajou University, Suwon 16499, Korea

[‡]CRI Center for Chemical Proteomics, Department of Chemistry and [§]Department of Biophysics and Chemical Biology, Seoul National University, Seoul 08826, Korea

Supporting Information

ABSTRACT: A facile turn-on chemical sensor array was developed for hydrazine detection by means of fluorescence pattern recognition. Taking advantage of the unique properties of the azo group, four different fluorogenic probes, Seoul-Fluor (SF)-Azo **01**−**04**, were designed and prepared. SF-Azo **01**−**04** displayed fluorescence enhancement of up to 800-fold upon reaction with hydrazine, and all probes exhibited excellent selectivity in the presence of various anions and nucleophiles. By employing the probes in a cellulose paper-based array system, the hydrazine concentration was successfully determined by monitoring the change in fluorescent patterns.

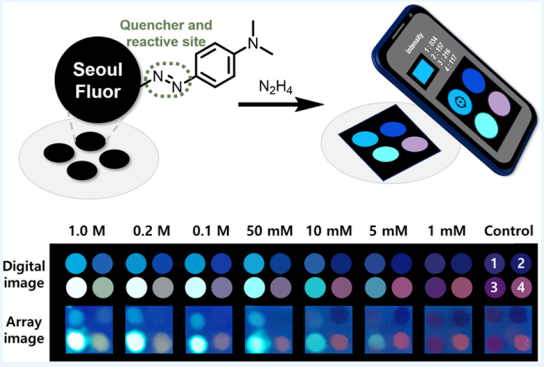

1. INTRODUCTION

Hydrazine, which possesses two single-bonded nucleophilic nitrogen atoms, exhibits ambivalent chemical behavior. It is known as a fuel propellant for rockets and spacecraft and has been widely used in diverse research areas, including pharmaceutical chemistry, agricultural chemistry, and coordination chemistry.[1−4] However, the U.S. Environmental Protection Agency (EPA)[5] classifies hydrazine as a toxic and carcinogenic chemical that damages the liver, kidneys, and central nervous system.[6] Further, high concentrations of hydrazine vapor have caused catastrophic explosions at chemical facilities. Therefore, in line with increasing biohazard risks and environmental safety concerns, attention is directed toward the development of selective detection methods for hydrazine species.

Various analytical techniques can be applied for the detection of hydrazine molecules, such as spectrophotometry,[7] titrimetry,[8,9] voltammetry,[10,11] and chromatography.[12,13] Among these, fluorescence techniques have multiple advantages over others, including sensitivity, immediacy, and easy accessibility.[14] Despite several enthusiastic efforts,[15−23] it is very difficult and laborious to develop highly selective and sensitive fluorogenic probe for certain analytes, such as hydrazine. On the other hand, optical array with chemoresponsive colorants could provide more sensitive and selective chemical sensing system via making use of pattern recognition of the combined response of chemoresponsive colorants, as our olfactory system.[24] We hypothesized that the development of fluorescent sensor arrays with more specific chemoresponsive colorant could increase the fidelity of molecular recognition of the system even further by taking advantage of their discriminatory powers.[25]

In the present study, we developed a chemical array system for hydrazine detection using fluorescent pattern analysis. Instead of using reported reaction-based electrophilic groups,[26−28] we focused on the azo group—a fluorescence quencher—and its reducing reaction mediated by hydrazine, due to its general applicability to a turn-on array system. To generate the components of an array system for hydrazine detection, we developed four different fluorogenic probes, SF-Azo **01**−**04**, by introducing an azo moiety on a versatile fluorescent molecular framework, 9-aryldihydropyrrolo[3,4-*b*]indolizin-3-one (Seoul-Fluor; hereafter SF).[29] We confirmed that the azo functional group successfully quenches the fluorescence of the SF system and that the reaction of the SF-Azo probes with hydrazine promotes fluorescence enhancement of up to 800-fold. Furthermore, simple spotting of SF-Azo compounds on a cellulose paper allowed us to set up a disposable facile 2 × 2 fluorescent sensor array. We could successfully detect and discriminate the concentration of hydrazine samples with the fluorescent array. This proof-of-concept study not only demonstrated the usefulness of the underevaluated azo functional group for hydrazine detection but, more importantly, it validated the practicality of using the fluorescent array system for sensing molecules of interest.

Received: May 21, 2019
Accepted: August 16, 2019
Published: September 3, 2019

Downloaded via AJOU UNIV on May 22, 2025 at 08:16:36 (UTC).
See https://pubs.acs.org/sharingguidelines for options on how to legitimately share published articles.

© 2019 American Chemical Society

DOI: 10.1021/acsomega.9b01487
ACS Omega 2019, 4, 14875−14885

2. RESULTS AND DISCUSSION

2.1. Design and Synthesis of Azo-Based Fluorescent Probes for Hydrazine Detection. Given the strong nucleophilicity of hydrazine, electrophilic moieties such as acetyl,[27,30−33] malononitrile,[28,34,35] and vinyl ketone[36] have been considered for preparing the reaction-based fluorescent sensors for hydrazine detection. However, most reactive groups simply induce a spectral shift upon hydrazine reaction and do not guarantee on/off-type fluorescence conversion, which is highly desirable for sensing and assay purposes.[37] Therefore, we focused on the azo group due to its dual functionality as a reactive unit for hydrazine[38−40] as well as a universal fluorescence quencher.[41,42] A small number of azo-based hydrazine sensors have been reported,[43,44] but the main interests lie in specific probe aggregates or the macroscopic behavior of the reaction products. Therefore, questions remain regarding azo-based common fluorophores and their on/off behavior as a general hydrazine sensor. As a fluorescent reporter system, we chose the SF system, which has proven to be a dynamic molecular platform exhibiting versatile changes in photophysical properties in response to target analytes or changes in the surrounding environment.[29] In addition, we unveiled the structure−photophysical property relationship of the Seoul-Flour skeleton, which allows easy tuning of its emission wavelengths.[45] Therefore, we envisioned the azo-embedded SF system (SF-Azo) as highly efficient fluorogenic turn-on hydrazine probes (Figure 1a). The emission color tenability of the SF system might provide a multicolor molecular set for the development of a fluorescent sensor system generating divergent patterns.

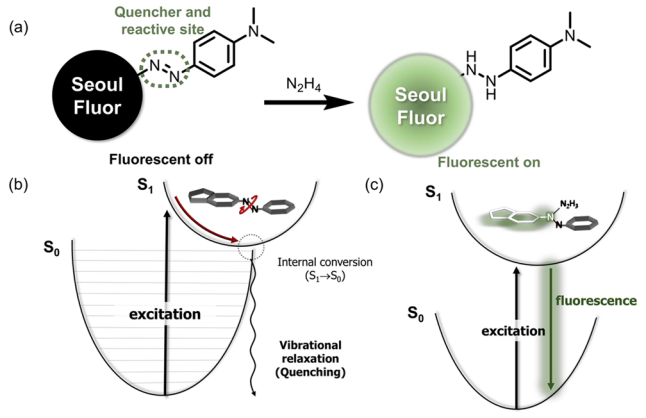

Figure 1. (a) Schematic of fluorogenic SF-Azo system for the detection of hydrazine. (b, c) Plausible photodeactivation processes for (b) SF-Azo compounds and (c) corresponding products after reaction with hydrazine.

A plausible mechanism of the fluorescence on/off phenomenon for the SF-Azo system is as follows. Mounting evidence suggests that after the photoexcitation of an azo-embedded π-conjugation system, the excitation energy easily dissipates through nonradiative S1 → S0 internal conversion because the π-bond in an azo group is involved in CN═NC bond rotation at the S1 state, making the energy barrier between the S1 state and the S0 state negligible.[46,47] Therefore, this excitation energy is efficiently transferred to the higher-lying S0 vibrational state, resulting in nonradiative energy decay through vibrational relaxation (Figure 1b). However, after the reaction with hydrazine molecules, the product loses its π-bond on the azo group, and consequently, the cis−trans isomerization at the excited state no longer exists. In this situation, the product loses its excited energy via the conventional deactivation pathway of the indolizine-based system (Figure 1c).

In our previous tetrazine-quencher study using the SF platform, more effective quenching was achieved when the quencher was directly installed on the indolizine core skeleton.[48] Therefore, we designed SF-Azo **01**−**03** as efficient fluorogenic hydrazine sensors with different fluorescent emission colors, promoted by three different functional groups: hydro, dimethylamino, and cyano groups for SF-Azo **01**, **02**, and **03**, respectively (Figure 2). Next, we considered that after the reduction of an azo group, a newly generated hydrazine moiety in the SF system should act as an electron-donating group (Figure 1a)[49] with a huge influence on the fluorescence property of the turn-on SF-Azo products. Since the SF system has previously shown a drastic bathochromic shift when forged with a pendent aniline moiety,[45] we additionally designed SF-Azo **04**, bearing a latent aniline moiety, to cover a longer emission wavelength. Consequently, we designed a multicolor set of fluorescent SF-Azo **01**−**04** for a series of fluorogenic hydrazine sensors.

For the synthesis of SF-Azo **01**−**03**, the most challenging step was 1,3-dipolar cycloaddition between the azo-pyridine and the alkyne substrate (Scheme 1). It is worth mentioning that after exhaustive screening of the reaction conditions for this step, we found that a copper source was essential for securing the desired azo-indolizine scaffold, but no desired products were obtained with other metals or halide sources. After further optimization (see Table S1), copper iodide and 1,8-diazabicyclo[5.4.0]undec-7-ene (DBU) in *N*,*N*-dimethylformamide (DMF) solvent were selected for synthesizing the azo-indolizine intermediate, **S1**, via 1,3-dipolar cycloaddition. Simple iodination, followed by palladium-mediated cross-coupling reaction allowed the synthesis of **S3**−**S5** with reasonable isolation yields (Scheme 1 and Supporting Information). For SF-Azo **04**, a reported synthetic strategy, i.e., palladium-mediated C−H bond coupling reaction,[50]

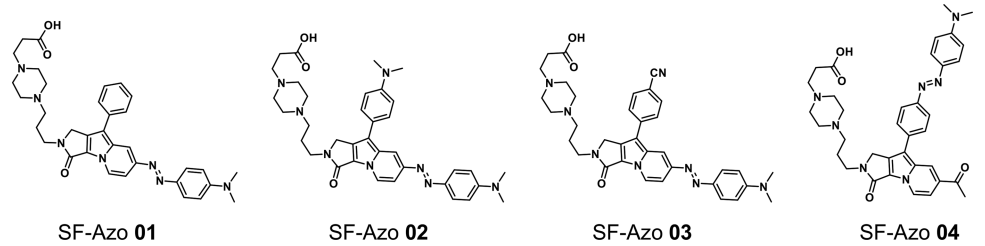

Figure 2. Chemical structures of SF-Azo **01**−**04**.

DOI: 10.1021/acsomega.9b01487
ACS Omega 2019, 4, 14875−14885

Scheme 1. Synthesis of SF-Azo 01−04

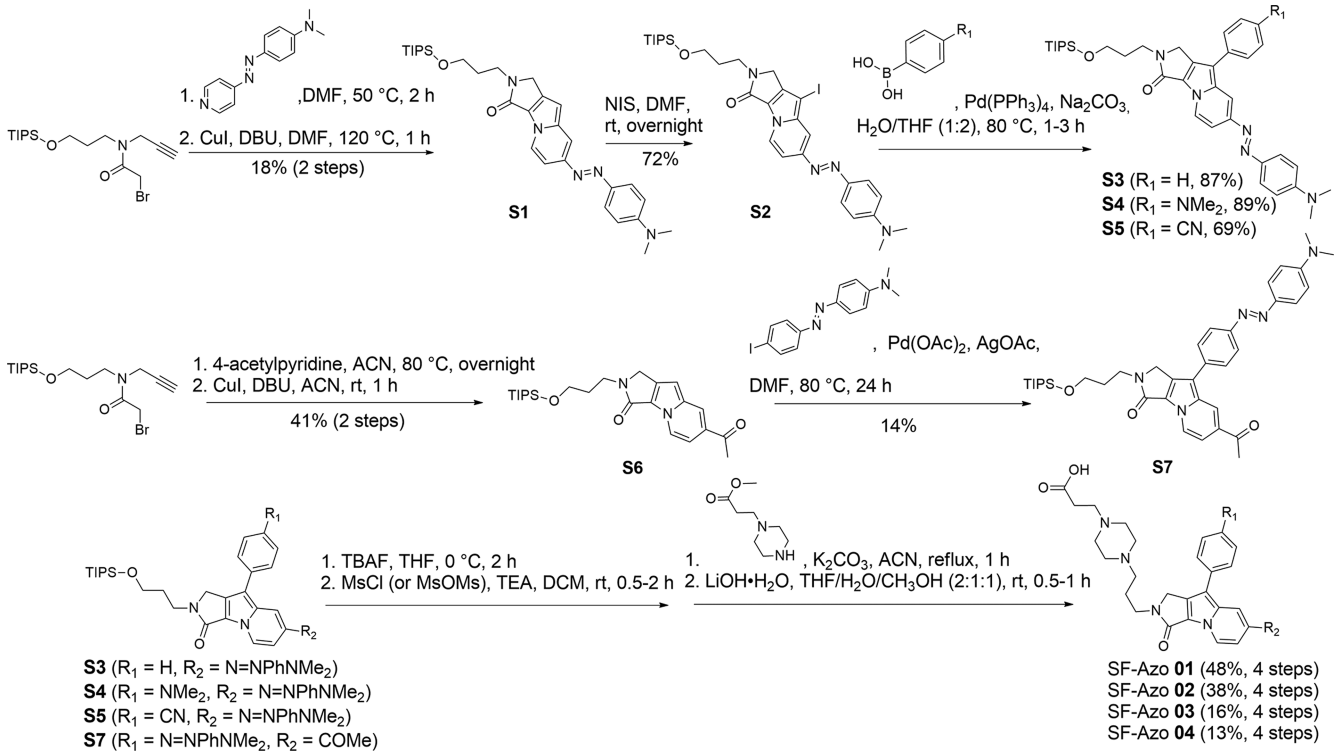

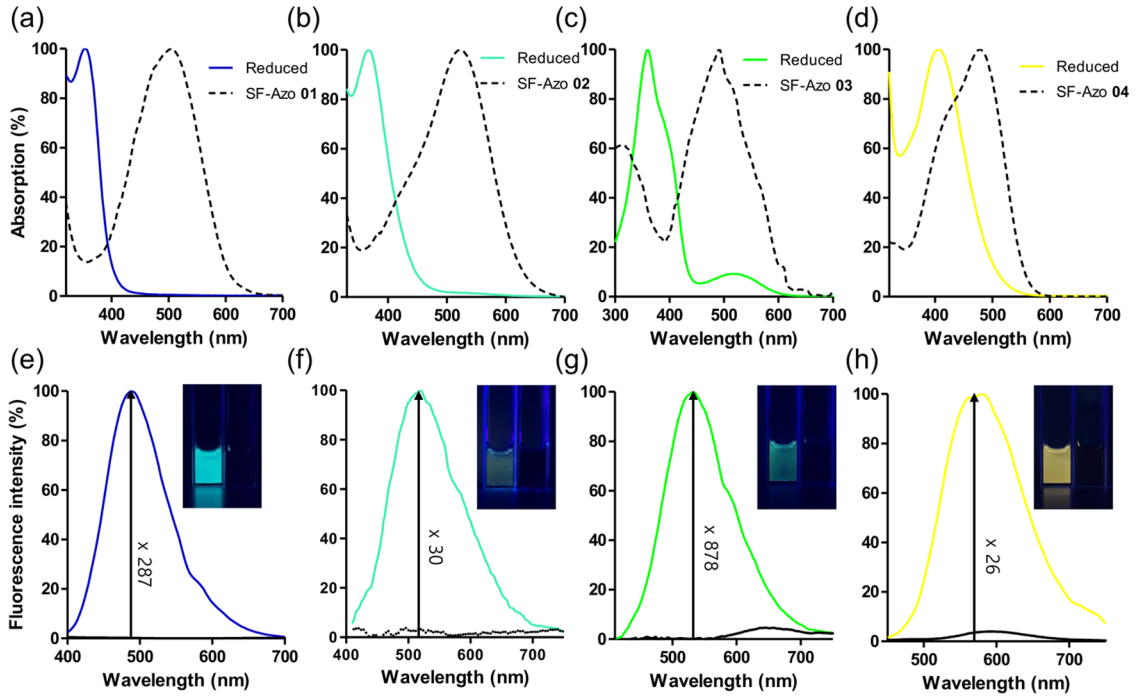

Figure 3. Changes in absorption (a−d) and emission spectra (e−h) for SF-Azo **01**−**04** (5 μM) before (black line) and after (colored line) the addition of hydrazine (200 mM): (a, e) SF-Azo **01**, (b, f) SF-Azo **02**, (c, g) SF-Azo **03**, and (d, h) SF-Azo **04**. Each probe was excited at the maximum absorption wavelength in a CH_3OH/H_2O (v/v = 1:1, 5 μM) mixture, and the inset photos (e−h) show the fluorogenic changes induced by hydrazine treatment, under a 365 nm handheld UV lamp.

allowed efficient synthesis of the desired intermediate, **S7**. Since we found that **S3**−**S5**, and **S7** are hardly soluble in polar solvents (having high cLog *P* values, ranging from 9.5 to 10.2; Figure S1), we replaced the triisopropylsilyl group with 3-(piperazin-1-yl)propanoic acid, which has shown its practicality through a previous application,[48] as a water-soluble moiety, to increase the aqueous solubility (cLog *P* values from 2.4 to 3.1) to detect hydrazine in water, and labeled them as SF-Azo **01**, **02**, **03**, and **04**, respectively.

2.2. Spectral Changes of SF-Azo 01−04 upon Chemoselective Reaction with Hydrazine. With the four newly designed SF-Azo compounds in hand, we investigated

DOI: 10.1021/acsomega.9b01487
ACS Omega 2019, 4, 14875−14885

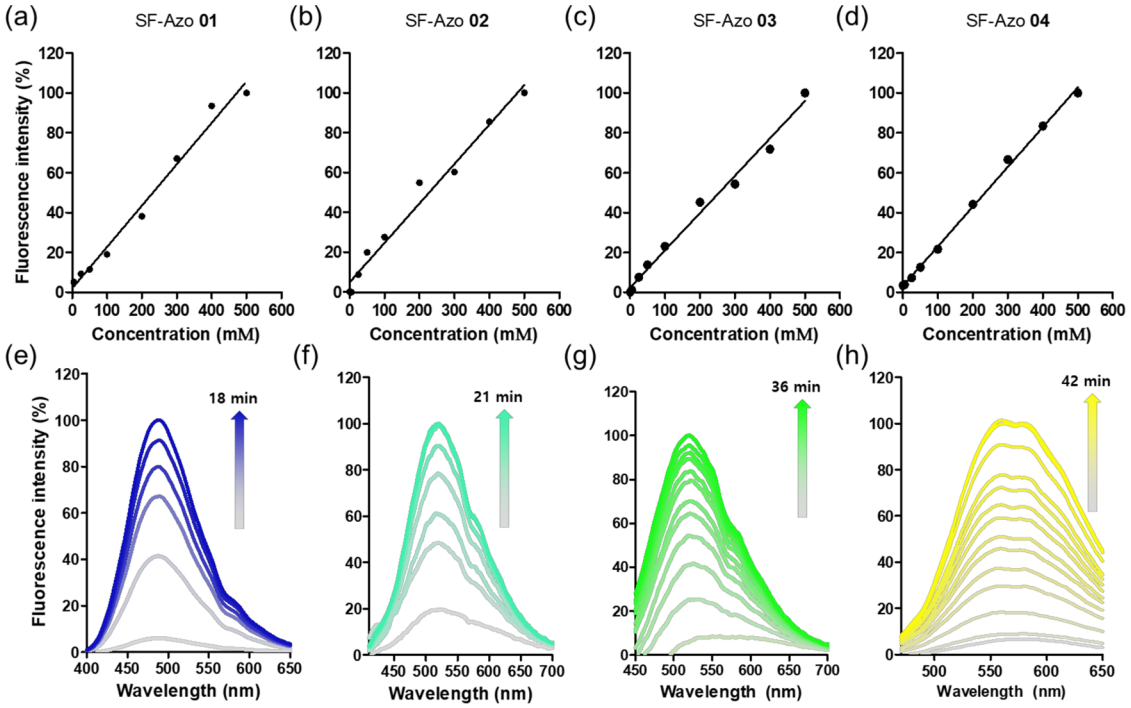

Figure 4. (a–d) Concentration- and (e–h) time-dependent changes in fluorescence intensity for SF-Azo **01**–**04** after the addition of hydrazine (200 mM): (a, e) SF-Azo **01**, (b, f) SF-Azo **02**, (c, g) SF-Azo **03**, and (d, h) SF-Azo **04**. Each probe was excited at the maximum absorption wavelength in a CH_3OH/H_2O (v/v = 1:1, 5 μM) mixture.

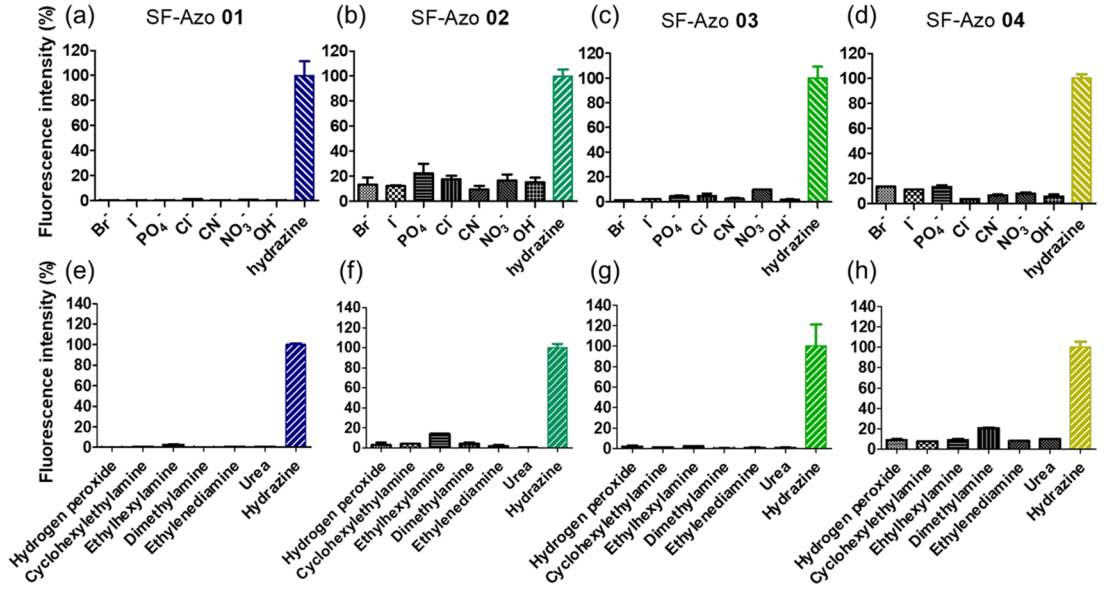

Figure 5. Fluorescence response of SF-Azo **01** (a, e), SF-Azo **02** (b, f), SF-Azo **03** (c, g), and SF-Azo **04** (d, h) in a CH_3OH/H_2O (v/v = 1:1, 5 μM) mixture upon the addition of 200 mM anions (Br^-, I^-, PO_4^{3-}, Cl^-, CN^-, NO_3^-, OH^-) and nucleophiles (hydrogen peroxide, cyclohexylethylamine, ethylhexylamine, dimethylamine, ethylenediamine, urea) compared with hydrazine. Fluorescence intensity changes against the treatment of other anions and nucleophiles were normalized against that of hydrazine. Each probe was excited at the maximum absorption wavelength.

the changes in the UV–vis spectra for the SF-Azo compounds in the absence and presence of hydrazine. As shown in Figure 3a–d, all of the compounds exhibited drastic hypsochromic shifts in the absorption spectra upon treatment with hydrazine; the maximum absorption wavelengths of SF-Azo **01**, **02**, **03**, and **04** changed from 506, 522, 492, and 478 nm to 350, 370, 360, and 410 nm, respectively. This result indicated that the π-conjugation system of SF-Azo **01**–**04** was reduced after the reaction with hydrazine, and the electronic states of the CN═NC bond-embedded SF-Azo compounds were completely different from those of the corresponding reduced products having a CNH–HNC single bond. To confirm this plausible mechanism, we incubated the SF-Azo **01** with hydrazine and monitored the resulting reaction mixture with liquid chromatography–mass spectrometry (LC–MS) after 5, 10, and 20 min incubation. Although we confirmed that mass value

DOI: 10.1021/acsomega.9b01487
ACS Omega 2019, 4, 14875–14885

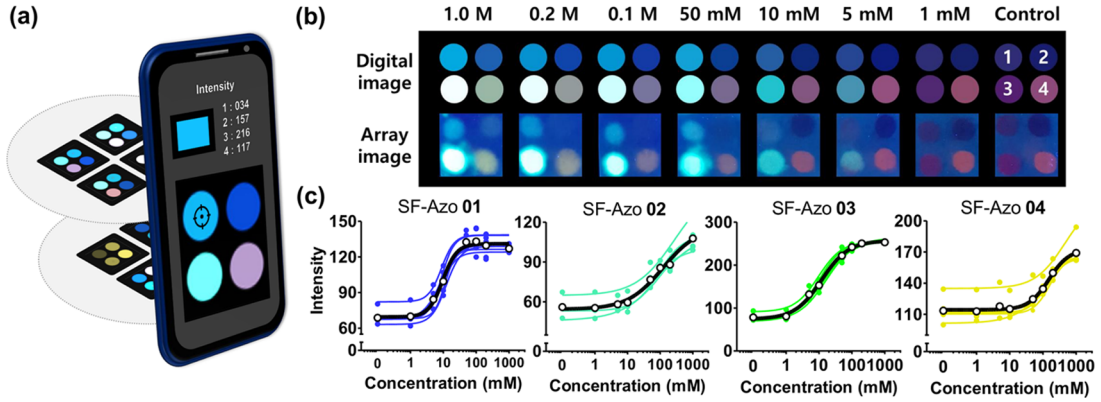

Figure 6. (a) Schematic representation of smartphone-based hydrazine sensing via capturing fluorescence images from a set of the array system. (b) Concentration-dependent changes in the fluorescence array pattern under a 365 nm handheld UV lamp (array image) and extracted color images using ImageJ (digital image); 1: SF-Azo **01**, 2: SF-Azo **02**, 3: SF-Azo **03**, 4: SF-Azo **04**. (c) Scatter plots of the fluorescence intensity and hydrazine concentration for individual probes comprising a set of the array system. Average intensity (solid line) was obtained from six independent experiments.

of single-bond reduction product (Figure S3), the mass value of an indolizine product without an aniline moiety was detected as well. Therefore, further study is in due course to address the exact mechanism of the chemical transformation.

After observing the absorption changes, we evaluated the turn-off (before reduction) and turn-on (after reduction) fluorescence properties for SF-Azo **01**−**04**. Not only SF-Azo **01**−**03** but also SF-Azo **04** showed a negligible background signal at the off state, before the reaction with hydrazine (Figure 3e−h). In contrast, the SF-Azo **01**−**04** probes displayed strong enhancement of fluorescence intensity (I/I_0 = 287-, 30-, 878-, and 26-fold, respectively) upon reaction with hydrazine, together with various emission maxima at 488, 520, 522, and 580 nm, respectively (Figure 3e−h). Therefore, these results clearly demonstrate that the SF-Azo system can serve as a highly efficient fluorogenic hydrazine reporter with multiple emission colors.

Next, we evaluated the factors affecting the fluorescence intensity of the four SF-Azo probes, such as the concentration of hydrazine and the incubation time with hydrazine. Figure 4a−d shows that all of the four fluorescent hydrazine sensors displayed dose-dependent fluorescence response according to the hydrazine concentration, implying that SF-Azo probes could be used as quantitative reporters in response to hydrazine concentration. We also checked the changes in fluorescence intensity over hydrazine incubation time (Figure 4e−h) and found that SF-Azo **01** showed the most rapid reaction kinetics with hydrazine, followed by **02**, **03**, and **04**.

2.3. Chemoselectivity Evaluation for SF-Azo 01−04. To assess the chemoselectivity of SF-Azo toward hydrazine, we investigated the effect of other chemical species, such as halides, phosphate, cyanide, nitrate, and other nucleophiles, on the fluorescence emission of the SF-Azo probes. We incubated 200 mM miscellaneous competing species (Br^-, I^-, PO_4^{3-}, Cl^-, CN^-, NO_3^-, OH^-) or hydrazine monohydrate with fluorogenic SF-Azo probes in a CH_3OH/H_2O (v/v = 1:1) mixture and monitored the changes in fluorescence intensity at the maximum emission wavelength of each probe (Figure 5). In addition, we incubated the SF-Azo probes with other nucleophiles (200 mM), such as hydrogen peroxide, cyclohexylethylamine, ethylhexylamine, dimethylamine, ethylenediamine, or urea, in a CH_3OH/H_2O (v/v = 1:1) mixture. To our pleasant surprise, all of the SF-Azo probes exhibited excellent chemoselectivity to hydrazine without any significant perturbation by other chemical species even at high concentrations (Figure 5). It is worth mentioning that Azo-SF **01** and **03** exhibited better selectivity than **02** and **04**. Presumably, this is due to the outstanding turn-on/-off ratio of Azo-SF **01** and **03** (Figure 3e−h), suggesting the importance of highly efficient turn-on fluorescence probes with minimized background noise. Overall, this result demonstrated the usefulness of the azo functional group as a selective chemical unit for reaction-based hydrazine sensing.

2.4. Application to Paper Array System for the Detection of Hydrazine. Finally, we applied our SF-Azo probes to develop a convenient and easily accessible fluorescence sensor array for hydrazine detection (Figure 6a). First, simple spotting of 1 mM methanol solution of SF-Azo probes on cellulose filter paper, followed by drying, allowed facile preparation of the 2 × 2 fluorescent chemical array. After the treatment of aqueous hydrazine solution on the designated spots, the array paper was heated at 75 °C for 30 min and the fluorescence change was monitored under a 365 nm UV lamp. Fluorescent patterns in the resulting paper arrays depending on various hydrazine concentrations (from 1.0 to 0.2, 0.1, 0.05, 0.01, 0.005, and 0.001 M) were captured using a smartphone camera (Figure 6b, array image). To analyze the pattern changes, color information of the array was extracted using the ImageJ program (Figure 6b, digital image). As shown in Figure 6c, the combination of four different multicolor fluorogenic SF-Azo probes in the array exhibited different fluorescence patterns depending on the concentration of hydrazine. The inflection point of the sigmoid curves for each turn-on probe was recorded as 9.7, 119.5, 12.1, and 151.1 mM for SF-Azo **01**, **02**, **03**, and **04**, respectively (Figure 6c). The limit of detection of the hydrazine sensor was confirmed to be 2.33 mM (limit of detection = blank signal + 3 standard deviation).[51,52] This is a much higher value than 10 ppb, low threshold limit of hydrazine from U.S. EPA. Further studies are in due course to decrease the detection limit of the system. To sum up, by taking advantage of the multiemission property of the SF-Azo system, not only the presence of hydrazine but also its concentration could be easily monitored by a user-friendly array system.

DOI: 10.1021/acsomega.9b01487
ACS Omega 2019, 4, 14875−14885

3. CONCLUSIONS

In this study, we focused on the azo functional group for the selective detection of hydrazine species. By taking advantage of its dual functionality as a fluorescence quencher and chemoselective reactivity with hydrazine, we successfully developed a series of reaction-based fluorogenic probes, SF-Azo **01**−**04**, to monitor hydrazine in a multicolor format. These probes exhibited a high fluorogenic turn-on ratio up to 878-fold upon reaction with hydrazine, as well as excellent chemoselectivity for hydrazine over other anions and nucleophiles. For convenient application, we generated the disposable paper array system, which can effectively determine hydrazine concentration simply by monitoring the pattern changes in the fluorescence emission color. Compared to conventional other analytical methods, generally requiring the sophisticated analytical instruments, recognition of simple fluorescent pattern changes of the array system allowed highly selective hydrazine chemical sensing system. Therefore, this proof-of-concept study demonstrate that fluorescent array system could provide easier and efficient way to develop highly selective chemical sensing system, such as hydrazine.

For further expansion of azo-fluorophores with greater hydrazine sensitivity, it is necessary to consider the reactivity change of azo groups to hydrazine. It is reported that aryl azo compounds have different reaction rates with hydrazine, depending on the substituents of azo compounds.[53,54] Therefore, the electronic nature of aromatic groups connected with an azo bond could be a critical factor for hydrazine sensitivity. Electron-deficient aromatic groups, such as pyridine, pyrimidine, or triazine, might be suitable candidates for general azo-fluorophores with improved hydrazine sensitivity.

4. EXPERIMENTAL SECTION

4.1. Compound Characterization. ^{1}H and ^{13}C NMR spectra were recorded on Agilent 400-NMR (Agilent Technologies), and Varian Inova-500 (Varian Associates). Chemical shifts were reported in parts per million (δ) and calibrated using internal tetramethylsilane standard or residual undeuterated solvent for ^{1}H NMR spectra ($CDCl_3$ 7.26 ppm) and for ^{13}C NMR spectra ($CDCl_3$ 77.16 ppm). Multiplicity was indicated as follows: s (singlet); d (doublet); t (triplet); q (quartet); quin (quintet); m (multiplet); dd (doublet of doublet); brs (broad singlet); etc. Coupling constants were reported in hertz (Hz). Low-resolution mass spectrometry (LRMS) was achieved by LCMS-2020 (Shimadzu). High-resolution mass spectrometry (HRMS) of compounds was further confirmed by ultra-high-resolution electrospray-ionization (ESI) quadrupole time-of-flight mass spectrometer (Bruker) from Organic Chemistry Research Center at Sogang University. Purity of SF-Azo compounds was confirmed using modular high-performance liquid chromatography (HPLC) prominence (Shimadzu).

4.2. Materials. All chemicals were purchased from Sigma-Aldrich, Tokyo Chemical Industry Co., Ltd., Alfa Aesar, or ThermoFisher Scientific and used without further purification unless otherwise specified. The progress of the reaction was monitored using thin-layer chromatography (TLC) (silica gel 60, F_{254} 0.25 mm), and components were visualized by observation under UV light (254 and 365 nm) or by treating the TLC plates with either *p*-anisaldehyde, $KMnO_4$ or ninhydrin followed by heating. Solvents were purchased from commercial venders and used without further purification. Filter papers (Catalog Number 1004-110) were purchased from Whatman.

4.3. Absorption and Fluorescence Measurement. Absorption and fluorescence emission spectra were recorded on SpectraMax iD5 multimode microplate reader. All experiments in microplate reader were performed in 96-well black well/clear bottom plate. The 96-well microplates were purchased from SPL. Absorption for molar absorptivity measurement was recorded on a JASCO V-770 spectrophotometer with a 1 × 1 cm^2 quartz cuvette.

4.4. Synthetic Procedure and Characterization of New Compounds. *4.4.1. Compound* ***S1***. (*E*)-*N*,*N*-Dimethyl-4-(pyridin-4-yldiazenyl)aniline[55] (432 mg, 1.91 mmol) and 2-bromo-*N*-(prop-2-yn-1-yl)-*N*-(3-((triisopropylsilyl)oxy)-propyl)-acetamide[48] (850 mg, 2.18 mmol) were dissolved in *N*,*N*-dimethylformamide (DMF, 2 mL). The solution was stirred at 50 °C for 2 h. After additional 10 mL of DMF was added, the mixture was heated to 120 °C. Then, copper iodide (363.6 mg, 1.91 mmol) and 1,8-diazabicyclo[5.4.0]undec-7-ene (DBU, 855 μL, 5.73 mmol) were added to the mixture and stirred for another 1 h at 120 °C. The mixture was filtered through a short bed of silica gel and concentrated under reduced pressure. The crude product was purified by flash column chromatography (silica gel, toluene/ethyl acetate = 10:1) to afford **S1** (178 mg, 334 μmol, 17.5% yield) as a red solid; ^{1}H NMR (400 MHz, $CDCl_3$) δ 8.52 (d, J = 7.3 Hz, 1H), 7.98 (brs, 1H), 7.87 (d, J = 9.3 Hz, 2H), 7.40 (dd, J = 7.6, 1.7 Hz, 1H), 6.77 (d, J = 9.3 Hz, 2H), 6.55 (s, 1H), 4.38 (s, 2H), 3.80 (t, J = 6.1 Hz, 2H), 3.69 (t, J = 7.3 Hz, 2H), 3.10 (s, 6H), 1.93 (quin, J = 6.8 Hz, 2H), 0.97−1.16 (m, 21H); ^{13}C NMR (100 MHz, $CDCl_3$) δ 161.8, 152.4, 146.0, 143.6, 139.8, 136.7, 125.2, 124.9, 122.6, 119.0, 111.5, 102.7, 96.93, 96.89, 60.9, 46.9, 40.3, 32.2, 18.0, 11.9; HRMS (ESI) m/z calcd for $C_{30}H_{44}N_5O_2Si$; $[M + H]^+$: 534.3259, found: 534.3260.

4.4.2. Compound ***S2***. **S1** (55.0 mg, 103 μmol) and *N*-iodosuccinimide (25.5 mg, 113 μmol) were dissolved in DMF (1 mL). The mixture was stirred at room temperature for 1 day. The crude product was directly purified by flash column chromatography (silica gel, toluene/ethyl acetate = 10:1) to afford **S2** (49.0 mg, 74.3 μmol, 72.1% yield) as a red solid; ^{1}H NMR (500 MHz, $CDCl_3$) δ 8.49 (d, J = 7.3 Hz, 1H), 7.93 (d, J = 2.0 Hz, 1H), 7.88 (d, J = 8.8 Hz, 2H), 7.43 (dd, J = 7.3, 2.0 Hz, 1H), 6.75 (d, J = 9.3 Hz, 2H), 4.27 (s, 2H), 3.80 (t, J = 6.1 Hz, 2H), 3.69 (t, J = 7.1 Hz, 2H), 3.10 (s, 6H), 1.92 (quin, J = 6.8 Hz, 2H), 0.98−1.20 (m, 21H); ^{13}C NMR (125 MHz, $CDCl_3$) δ 161.4, 152.7, 147.2, 143.7, 141.1, 140.1, 125.94, 125.92, 125.3, 124.2, 118.5, 111.7, 103.8, 61.1, 48.7, 47.2, 40.6, 40.4, 32.2, 18.2, 12.1; HRMS (ESI) m/z calcd for $C_{30}H_{43}IN_5O_2Si$; $[M + H]^+$: 660.2225, found: 660.2226.

4.4.3. Compound ***S3***. **S2** (200 mg, 303 μmol), phenylboronic acid (111 mg, 910 μmol), tetrakis(triphenylphosphine)palladium(0) ($Pd(PPh_3)_4$, 70.1 mg, 60.6 μmol), and sodium carbonate (160.7 mg, 1.52 mmol) were dissolved in a mixture of water (1 mL) and tetrahydrofuran (THF, 2 mL). The mixture was stirred at 80 °C for 2 h. After full consumption of the starting material monitored by TLC, the mixture was filtered through a short bed of silica gel and resulting residue was washed with saturated $NaHCO_3$ aqueous solution, extracted with ethyl acetate, dried over anhydrous Na_2SO_4, and concentrated. The crude product was purified by flash column chromatography (silica gel, toluene/ethyl acetate = 40:1) to afford **S3** (160.8 mg, 263.7 μmol, 87.0% yield) as a

DOI: 10.1021/acsomega.9b01487
ACS Omega 2019, 4, 14875−14885

red solid; ^{1}H NMR (400 MHz, $CDCl_3$) δ 8.54 (d, J = 7.4 Hz, 1H), 8.32 (s, 1H), 7.86 (d, J = 9.0 Hz, 2H), 7.62 (d, J = 7.4 Hz, 2H), 7.48 (t, J = 7.8 Hz, 2H), 7.43 (dd, J = 7.4, 1.6 Hz, 1H), 7.31 (t, J = 7.0 Hz, 1H), 6.74 (d, J = 9.0 Hz, 2H), 4.53 (s, 2H), 3.81 (t, J = 6.1 Hz, 2H), 3.72 (t, J = 7.2 Hz, 2H), 3.08 (s, 6H), 1.94 (quin, J = 6.6 Hz, 2H), 0.93−1.18 (m, 21H); ^{13}C NMR (100 MHz, $CDCl_3$) δ 161.8, 152.5, 147.0, 143.8, 136.4, 135.1, 134.4, 129.2, 127.4, 126.3, 125.7, 125.1, 122.7, 119.1, 112.6, 111.7, 103.0, 61.1, 47.3, 40.5, 40.4, 32.3, 18.2, 12.1; HRMS (ESI) m/z calcd for $C_{36}H_{48}N_5O_2Si$ $[M + H]^+$: 610.3572, found: 610.3574.

4.4.4. Compound ***S4****.* **S2** (220 mg, 333.5 μmol), 4-(dimethylamino)phenylboronic acid (165 mg, 1.00 mmol), $Pd(PPh_3)_4$ (77.1 mg, 66.7 μmol), and sodium carbonate (177 mg, 1.67 mmol) were dissolved in a mixture of THF (300 μL) and water (150 μL). The mixture was stirred at 80 °C for 1 h. After full consumption of the starting material monitored by TLC, the mixture was filtered through a short bed of silica gel and the resulting residue was washed with saturated $NaHCO_3$ aqueous solution, dried over anhydrous Na_2SO_4, and concentrated. The crude product was purified by flash column chromatography (silica gel, toluene/ethyl acetate = 20:1) to afford **S4** (194 mg, 297 μmol, 89.1% yield) as a red solid; ^{1}H NMR (400 MHz, $CDCl_3$) δ 8.51 (d, J = 7.4 Hz, 1H), 8.31 (s, 1H), 7.86 (d, J = 9.0 Hz, 2H), 7.53 (d, J = 8.6 Hz, 2H), 7.40 (dd, J = 7.6, 1.8 Hz, 1H), 6.87 (d, J = 8.6 Hz, 2H), 6.76 (d, J = 9.4 Hz, 2H), 4.52 (s, 2H), 3.82 (t, J = 6.1 Hz, 2H), 3.72 (t, J = 7.0 Hz, 2H), 3.10 (s, 6H), 3.03 (s, 6H), 1.94 (quin, J = 6.7 Hz, 2H), 0.96−1.19 (m, 21H); ^{13}C NMR (100 MHz, $CDCl_3$) δ 161.8, 152.2, 149.1, 146.3, 143.7, 135.8, 134.3, 128.2, 125.4, 124.8, 122.4, 119.8, 113.2, 113.1, 111.6, 102.4, 77.2, 61.0, 47.1, 40.6, 40.4, 40.3, 32.2, 18.0, 12.0; HRMS (ESI) m/z calcd for $C_{38}H_{53}N_6O_2Si$ $[M + H]^+$: 653.3994, found: 653.3996.

4.4.5. Compound ***S5****.* **S2** (30.0 mg, 45.5 μmol), 4-cyanophenylboronic acid (20.1 mg, 136 μmol), $Pd(PPh_3)_4$ (10.5 mg, 9.10 μmol), and sodium carbonate (24.1 mg, 227 μmol) were dissolved in mixture of THF (300 μL) and water (150 μL). The mixture was stirred at 80 °C for 3 h. The resulting residue was washed with saturated $NaHCO_3$ aqueous solution, extracted with CH_2Cl_2, dried over anhydrous Na_2SO_4, and concentrated. The crude product was purified by flash column chromatography (silica gel, hexane/ethyl acetate = 2:1) followed by washing with ethyl ether to afford **S5** (19.9 mg, 31.3 μmol, 68.9% yield) as a red solid; ^{1}H NMR (400 MHz, $CDCl_3$) δ 8.60 (d, J = 7.4 Hz, 1H), 8.32 (s, 1H), 7.89 (d, J = 8.6 Hz, 2H), 7.76 (d, J = 8.2 Hz, 2H), 7.71 (d, J = 8.2 Hz, 2H), 7.51 (d, J = 7.4 Hz, 1H), 6.77 (d, J = 9.0 Hz, 2H), 4.58 (s, 2H), 3.82 (t, J = 5.7 Hz, 2H), 3.75 (t, J = 7.0 Hz, 2H), 3.12 (s, 6H), 1.95 (quin, J = 6.6 Hz, 2H), 0.95−1.23 (m, 21H); ^{13}C NMR (100 MHz, $CDCl_3$) δ 161.4, 152.7, 147.8, 143.5, 139.3, 136.9, 135.3, 132.9, 127.1, 125.9, 125.3, 123.2, 119.2, 117.8, 111.6, 110.2, 108.8, 103.7, 60.9, 47.3, 40.5, 40.3, 32.1, 18.0, 11.9; HRMS (ESI) m/z calcd for $C_{37}H_{47}N_6O_2Si$ $[M + H]^+$: 635.3524, found: 635.3525.

4.4.6. Compound ***S6****.* 2-Bromo-*N*-(prop-2-yn-1-yl)-*N*-(3-((triisopropylsilyl)oxy)propyl)acetamide (3.00 g, 7.68 mmol) and 4-acetylpyridine (1.12 g, 9.22 mmol) were dissolved in acetonitrile (8 mL). The mixture was stirred at 80 °C for overnight. After full consumption of the starting material monitored by TLC, additional 70 mL of acetonitrile was added to the mixture. Then, copper iodide (1.46 g, 7.68 mmol) and DBU (3.44 mL, 23.1 mmol) were added to the mixture and stirred for another 1 h at room temperature. The mixture was filtered through a short bed of silica gel and concentrated under reduced pressure. The crude product was purified by flash column chromatography (silica gel, hexane/ethyl acetate = 4:1) to afford **S6** (1.34 g, 3.13 mmol, 40.7% yield) as a yellowish solid; ^{1}H NMR (400 MHz, $CDCl_3$) δ 8.53 (d, J = 7.4 Hz, 1H), 8.12 (s, 1H), 7.24 (dd, J = 7.4, 1.6 Hz, 1H), 6.64 (s, 1H), 4.40 (s, 2H), 3.80 (t, J = 6.1 Hz, 2H), 3.70 (t, J = 7.2 Hz, 2H), 2.61 (s, 3H), 1.92 (quin, J = 6.7 Hz, 2H), 0.96−1.17 (m, 21H); ^{13}C NMR (100 MHz, $CDCl_3$) δ 195.7, 161.5, 137.8, 136.6, 128.4, 124.4, 123.6, 122.1, 108.9, 98.34, 98.31, 60.9, 46.9, 40.4, 32.1, 26.0, 18.0, 11.9; HRMS (ESI) m/z calcd for $C_{24}H_{36}N_2NaO_3Si$ $[M + Na]^+$: 451.2387, found: 451.2388.

4.4.7. Compound ***S7****.* **S6** (100 mg, 233 μmol), (*E*)-4-((4-iodophenyl)diazenyl)-*N*,*N*-dimethylaniline[56] (163.9 mg, 466.6 μmol), palladium acetate (10.5 mg, 46.7 μmol), and silver acetate (77.9 mg, 466.6 μmol) were dissolved in DMF (2.5 mL). The mixture was stirred at 80 °C for 24 h. The mixture was filtered through short bed of silica and concentrated under reduced pressure. The crude product was purified by flash column chromatography (silica gel, hexane/ethyl acetate = 2:1) to afford **S7** (21.4 mg, 32.8 μmol, 14.1% yield) as a red solid; ^{1}H NMR (500 MHz, $CDCl_3$) δ 8.58 (d, J = 7.3 Hz, 1H), 8.46 (s, 1H), 7.97 (d, J = 7.8 Hz, 2H), 7.90 (d, J = 8.8 Hz, 2H), 7.65 (d, J = 8.3 Hz, 2H), 7.29 (d, J = 7.3 Hz, 1H), 6.77 (d, J = 8.8 Hz, 2H), 4.59 (s, 2H), 3.82 (t, J = 5.9 Hz, 2H), 3.75 (t, J = 7.1 Hz, 2H), 3.10 (s, 6H), 2.62 (s, 3H), 1.95 (quin, J = 6.5 Hz, 2H), 0.97−1.16 (m, 21H); ^{13}C NMR (125 MHz, $CDCl_3$) δ 195.5, 161.3, 152.5, 151.7, 143.7, 135.0, 134.7, 134.5, 129.3, 127.8, 125.0, 124.7, 123.6, 123.2, 121.4, 113.6, 111.5, 109.6, 60.9, 47.2, 40.5, 40.3, 32.0, 26.1, 18.0, 12.0; HRMS (ESI) m/z calcd for $C_{38}H_{50}N_5O_3Si$ $[M + H]^+$: 652.3677, found: 652.3679.

4.4.8. Compound ***S8****.* **S3** (138 mg, 226 μmol) and tetrabutylammonium fluoride (TBAF) solution 1 M in THF (272 μL, 272 μmol) were dissolved in THF (2.3 mL). The mixture was stirred at 0 °C for 2 h. The crude product was directly purified by flash column chromatography (silica gel, CH_2Cl_2/CH_3OH = 40:1) to afford a red solid; LRMS (ESI) m/z calcd for $C_{27}H_{28}N_5O_2$ $[M + H]^+$: 454.22, found: 454.10. To a solution of resulting product and triethylamine (TEA, 158 μL, 1.13 mmol) in dichloromethane (2.3 mL), methanesulfonyl chloride (35 μL, 450 μmol) was added slowly. The mixture was stirred at room temperature for 0.5 h. The crude product was directly purified by flash column chromatography (silica gel, CH_2Cl_2/CH_3OH = 40:1) to afford **S8** (110.3 mg, 207.5 μmol, 91.7% yield) as a red solid; ^{1}H NMR (400 MHz, $CDCl_3$) δ 8.52 (d, J = 7.4 Hz, 1H), 8.33 (s, 1H), 7.87 (d, J = 8.6 Hz, 2H), 7.62 (d, J = 7.8 Hz, 2H), 7.39−7.56 (m, 3H), 7.28−7.38 (m, 1H), 6.76 (d, J = 9.0 Hz, 2H), 4.53 (s, 2H), 4.34 (t, J = 6.1 Hz, 2H), 3.74 (t, J = 6.5 Hz, 2H), 3.10 (s, 6H), 3.06 (s, 3H), 2.08−2.24 (m, 2H); ^{13}C NMR (100 MHz, $CDCl_3$) δ 161.9, 152.5, 147.0, 143.6, 136.7, 135.0, 134.0, 129.2, 127.3, 126.4, 125.6, 125.1, 121.8, 118.8, 112.6, 111.6, 103.2, 67.6, 47.0, 40.3, 39.6, 37.4, 28.7; LRMS (ESI) m/z calcd for $C_{28}H_{30}N_5O_4S$ $[M + H]^+$: 532.20, found: 532.25.

4.4.9. Compound ***S9****.* **S4** (61.9 mg, 94.8 μmol) and TBAF solution 1 M in THF (114 μL, 114 μmol) were dissolved in THF (950 μL). The mixture was stirred at 0 °C for 2 h. The crude product was directly purified by flash column chromatography (silica gel, CH_2Cl_2/CH_3OH = 60:1) to afford resulting red solid; LRMS (ESI) m/z calcd for $C_{29}H_{33}N_6O_2$ $[M + H]^+$: 497.27, found: 497.10. To a solution of resulting product and TEA (66 μL, 470 μmol) in dichloromethane (1

DOI: 10.1021/acsomega.9b01487
ACS Omega 2019, 4, 14875−14885

mL), methanesulfonyl chloride (14.7 μL, 190 μmol) was added slowly. The mixture was stirred at room temperature for 0.5 h. The crude product was directly purified by flash column chromatography (silica gel, CH_2Cl_2/CH_3OH = 40:1) to afford **S9** (47.8 mg, 83.2 μmol, 87.7% yield) as a red solid; ^{1}H NMR (400 MHz, $CDCl_3$) δ 8.46 (d, *J* = 7.4 Hz, 1H), 8.28 (s, 1H), 7.86 (d, *J* = 9.0 Hz, 2H), 7.49 (d, *J* = 8.6 Hz, 2H), 7.40 (dd, *J* = 7.4, 1.6 Hz, 1H), 6.86 (d, *J* = 8.6 Hz, 2H), 6.75 (d, *J* = 9.0 Hz, 2H), 4.47 (s, 2H), 4.33 (t, *J* = 6.3 Hz, 2H), 3.71 (t, *J* = 6.7 Hz, 2H), 3.09 (s, 6H), 3.05 (s, 3H), 3.02 (s, 6H), 2.14 (quin, *J* = 6.3 Hz, 2H); ^{13}C NMR (100 MHz, $CDCl_3$) δ 162.0, 152.3, 149.2, 146.5, 143.7, 136.2, 134.3, 128.2, 125.4, 124.9, 122.1, 121.6, 119.6, 113.4, 113.1, 111.6, 102.7, 67.7, 47.0, 40.6, 40.3, 39.6, 37.4, 28.7; LRMS (ESI) *m*/*z* calcd for $C_{30}H_{35}N_6O_4S$ $[M + H]^+$: 575.24, found: 575.05.

*4.4.10. Compound **S10**.* **S5** (61.2 mg, 96.4 μmol) and TBAF solution 1 M in THF (116 μL, 116 μmol) were dissolved in THF (800 μL). The mixture was stirred at 0 °C for 2 h. The crude product was directly purified by flash column chromatography (silica gel, CH_2Cl_2/CH_3OH = 60:1) to afford a red solid; LRMS (ESI) *m*/*z* calcd for $C_{28}H_{27}N_6O_2$ $[M + H]^+$: 479.22, found: 479.05. To a solution of resulting product and TEA (67.2 μL, 482 μmol) in dichloromethane (1 mL), methanesulfonyl chloride (14.9 μL, 193 μmol) was added slowly. The mixture was stirred at room temperature for 0.5 h. The crude product was directly purified by flash column chromatography (silica gel, CH_2Cl_2/CH_3OH = 40:1) to afford **S10** (34.0 mg, 61.1 μmol, 63.4% yield) as a red solid; ^{1}H NMR (400 MHz, $CDCl_3$) δ 8.52 (d, *J* = 7.4 Hz, 1H), 8.25 (s, 1H), 7.87 (d, *J* = 9.0 Hz, 2H), 7.74 (d, *J* = 7.8 Hz, 2H), 7.68 (d, *J* = 8.2 Hz, 2H), 7.47 (d, *J* = 7.0 Hz, 1H), 6.76 (d, *J* = 8.6 Hz, 2H), 4.53 (s, 2H), 4.34 (t, *J* = 5.9 Hz, 2H), 3.74 (t, *J* = 6.5 Hz, 2H), 3.11 (s, 6H), 3.06 (s, 3H), 2.18 (t, *J* = 6.1 Hz, 2H); ^{13}C NMR (100 MHz, $CDCl_3$) δ 161.6, 152.8, 148.0, 143.5, 139.0, 137.2, 135.4, 132.9, 127.2, 125.8, 125.4, 122.4, 119.1, 117.6, 111.6, 110.3, 109.0, 104.0, 67.5, 47.1, 40.3, 39.7, 37.5, 28.7; LRMS (ESI) *m*/*z* calcd for $C_{29}H_{29}N_6O_4S$ $[M + H]^+$: 557.20, found: 557.00.

*4.4.11. Compound **S11**.* **S7** (22.5 mg, 34.5 μmol) and TBAF solution 1 M in THF (51.8 μL, 51.8 μmol) were dissolved in THF (100 μL). The mixture was stirred at 0 °C for 1.5 h. The resulting residue was washed with saturated brine, extracted with CH_2Cl_2, dried over anhydrous Na_2SO_4, and concentrated; LRMS (ESI) *m*/*z* calcd for $C_{29}H_{30}N_5O_3$ $[M + H]^+$: 496.23, found: 496.20; The resulting crude solid, methanesulfonic anhydride (18.0 mg, 102 μmol), and TEA (48 μL, 340 μmol) were dissolved in CH_2Cl_2 (350 μL). The mixture was stirred at room temperature for 2 h. The crude product was directly purified by flash column chromatography (silica gel, CH_2Cl_2/CH_3OH = 60:1) to afford **S11** (15 mg, 26 μmol, 76% yield) as a red solid; ^{1}H NMR (500 MHz, $CDCl_3$) δ 8.55 (d, *J* = 7.4 Hz, 1H), 8.44 (s, 1H), 7.97 (d, *J* = 8.2 Hz, 2H), 7.90 (d, *J* = 9.0 Hz, 2H), 7.63 (d, *J* = 8.6 Hz, 2H), 7.30 (dd, *J* = 7.4, 1.6 Hz, 1H), 6.77 (d, *J* = 9.0 Hz, 2H), 4.57 (s, 2H), 4.34 (t, *J* = 6.1 Hz, 2H), 3.76 (t, *J* = 6.7 Hz, 2H), 3.10 (s, 6H), 3.07 (s, 3H), 2.62 (s, 3H), 2.11−2.26 (m, 2H); ^{13}C NMR (100 MHz, $CDCl_3$) δ 195.5, 161.6, 152.5, 151.8, 143.6, 135.0, 134.8, 134.4, 129.6, 127.8, 125.1, 124.7, 123.2, 122.8, 121.3, 113.7, 111.5, 109.8, 67.4, 47.0, 40.3, 39.6, 37.5, 28.6, 26.1; LRMS (ESI) *m*/*z* calcd for $C_{30}H_{32}N_5O_5S$ $[M + H]^+$: 574.21, found: 574.25.

*4.4.12. Compound SF-Azo **01**.* **S8** (44.5 mg, 83.7 μmol), methyl 3-(piperazin-1-yl)propanoate (100.5 mg, 251.1 μmol), and potassium carbonate (115.7 mg, 837.1 μmol) were dissolved in acetonitrile (0.8 mL). The mixture was stirred at reflux condition for 1 h. The resulting residue was washed with saturated $NaHCO_3$ aqueous solution, extracted with CH_2Cl_2, dried over anhydrous Na_2SO_4, and concentrated. The crude product was purified by flash column chromatography (silica gel, CH_2Cl_2/CH_3OH = 40:1−20:1) to afford **S8′** (34.0 mg, 55.9 μmol, 66.8% yield) as a red solid; ^{1}H NMR (400 MHz, $CDCl_3$) δ 8.54 (d, *J* = 7.4 Hz, 1H), 8.33 (s, 1H), 7.87 (d, *J* = 9.0 Hz, 2H), 7.63 (d, *J* = 7.4 Hz, 2H), 7.49 (t, *J* = 7.6 Hz, 2H), 7.45 (dd, *J* = 7.4, 1.6 Hz, 1H), 7.28−7.35 (m, 1H), 6.76 (d, *J* = 9.0 Hz, 2H), 4.50 (s, 2H), 3.55−3.75 (m, 5H), 3.08 (s, 6H), 2.68 (t, *J* = 7.4 Hz, 2H), 2.47 (dt, *J* = 14.7, 7.5 Hz, 12H), 1.89 (quin, *J* = 7.0 Hz, 2H); ^{13}C NMR (100 MHz, $CDCl_3$) δ 172.9, 161.8, 152.4, 147.0, 143.7, 136.4, 134.9, 134.3, 129.1, 127.3, 126.3, 125.6, 125.0, 122.4, 118.9, 112.5, 111.6, 103.0, 55.8, 53.5, 53.2, 52.8, 51.65 (rotamer A), 51.62 (rotamer B), 46.7, 41.3, 40.3, 32.0, 26.3; LRMS (ESI) *m*/*z* calcd for $C_{35}H_{42}N_7O_3$ $[M + H]^+$: 608.33, found: 608.20; **S8′** (9.9 mg, 16 μmol) and lithium hydroxide monohydrate (2.1 mg, 49 μmol) were dissolved in 200 μL of $THF/H_2O/CH_3OH$ = 2:1:1 (v/v/v) mixture. The reaction mixture was stirred at room temperature for 0.5 h. The crude product was directly purified by reverse-phase preparative HPLC using a linear gradient of acetonitrile (5−100%) in water with 0.1% TFA to afford TFA salts of SF-Azo **01** (11.8 mg, 12.6 μmol, 77.4% yield) as a red solid; HRMS (ESI) *m*/*z* calcd for $C_{34}H_{40}N_7O_3$ $[M + H]^+$: 594.3187, found: 594.3189.

*4.4.13. Compound SF-Azo **02**.* **S9** (46.0 mg, 80.0 μmol), methyl 3-(piperazin-1-yl)propanoate (96.1 mg, 240 μmol), and potassium carbonate (111 mg, 800 μmol) were dissolved in acetonitrile (0.8 mL). The mixture was stirred at reflux condition for 1 h. The resulting residue was washed with saturated $NaHCO_3$ aqueous solution, extracted with CH_2Cl_2, dried over anhydrous Na_2SO_4, and concentrated. The crude product was purified by flash column chromatography (silica gel, CH_2Cl_2/CH_3OH = 40:1−20:1) to afford **S9′** (32.2 mg, 49.5 μmol, 61.8% yield) as a red solid; ^{1}H NMR (400 MHz, $CDCl_3$) δ 8.50 (d, *J* = 7.4 Hz, 1H), 8.24−8.34 (m, 1H), 7.86 (d, *J* = 9.0 Hz, 2H), 7.51 (d, *J* = 8.6 Hz, 2H), 7.40 (dd, *J* = 7.6, 1.8 Hz, 1H), 6.87 (d, *J* = 9.0 Hz, 2H), 6.76 (d, *J* = 9.0 Hz, 2H), 4.47 (s, 2H), 3.56−3.74 (m, 5H), 3.09 (s, 6H), 3.03 (s, 6H), 2.68 (t, *J* = 7.4 Hz, 2H), 2.35−2.64 (m, 12H), 1.88 (quin, *J* = 7.1 Hz, 2H); ^{13}C NMR (100 MHz, $CDCl_3$) δ 172.9, 161.9, 152.3, 149.2, 146.4, 143.8, 135.9, 134.2, 128.2, 125.4, 124.9, 122.3, 122.2, 119.7, 113.3, 113.1, 111.6, 102.5, 55.8, 53.5, 53.2, 52.8, 51.7 (rotamer A), 51.6 (rotamer B), 46.7, 41.3, 40.6, 40.3, 32.0, 26.3; LRMS (ESI) *m*/*z* calcd for $C_{37}H_{47}N_8O_3$ $[M + H]^+$: 651.38, found: 651.15; **S9′** (11 mg, 17 μmol) and lithium hydroxide monohydrate (2.1 mg, 51 μmol) were dissolved in 200 μL of $THF/H_2O/CH_3OH$ = 2:1:1 (v/v/v) mixture. The reaction mixture was stirred at room temperature for 0.5 h. The crude product was directly purified by reverse-phase preparative HPLC using a linear gradient of acetonitrile (5−100%) in water with 0.1% TFA to afford TFA salts of SF-Azo **02** (11.4 mg, 11.7 μmol, 68.9% yield) as a red solid; HRMS (ESI) *m*/*z* calcd for $C_{36}H_{45}N_8O_3$ $[M + H]^+$: 637.3609, found: 637.3610.

*4.4.14. Compound SF-Azo **03**.* **S10** (33.5 mg, 60.2 μmol), methyl 3-(piperazin-1-yl)propanoate (72.3 mg, 181 μmol), and potassium carbonate (83.2 mg, 602 μmol) were dissolved in acetonitrile (0.6 mL). The mixture was stirred at reflux condition for 1 h. The resulting residue was washed with

DOI: 10.1021/acsomega.9b01487
ACS Omega 2019, 4, 14875−14885

saturated $NaHCO_3$ aqueous solution, extracted with CH_2Cl_2, dried over anhydrous Na_2SO_4, and concentrated. The crude product was purified by flash column chromatography (silica gel, CH_2Cl_2/CH_3OH = 40:1−20:1) to afford **S10′** (20.7 mg, 32.7 μmol, 54.4% yield) as a red solid; ^1H NMR (400 MHz, $CDCl_3$) δ 8.59 (d, *J* = 7.4 Hz, 1H), 8.31 (s, 1H), 7.89 (d, *J* = 9.0 Hz, 2H), 7.76 (d, *J* = 8.6 Hz, 2H), 7.71 (d, *J* = 8.2 Hz, 2H), 7.50 (dd, *J* = 7.4, 1.6 Hz, 1H), 6.77 (d, *J* = 9.4 Hz, 2H), 4.53 (s, 2H), 3.56−3.79 (m, 5H), 3.12 (s, 6H), 2.68 (t, *J* = 7.4 Hz, 2H), 2.47 (m, 12H), 1.90 (quin, *J* = 6.9 Hz, 2H); ^{13}C NMR (100 MHz, $CDCl_3$) δ 172.9, 161.4, 152.7, 147.9, 143.5, 139.2, 137.0, 135.3, 132.9, 127.1, 125.9, 125.3, 123.0, 119.2, 117.7, 111.6, 110.2, 108.9, 103.9, 55.7, 53.5, 53.1, 52.8, 51.7 (rotamer A), 51.6 (rotamer B), 46.8, 41.4, 40.3, 32.0, 26.2; LRMS (ESI) *m*/*z* calcd for $C_{36}H_{41}N_8O_3$ $[M + H]^+$: 633.33, found: 633.15. **S10′** (12.5 mg, 19.8 μmol) and lithium hydroxide monohydrate (2.5 mg, 59 μmol) were dissolved in 200 μL of THF/H_2O/CH_3OH = 2:1:1 (v/v/v) mixture. The reaction mixture was stirred at room temperature for 1 h. The crude product was directly purified by reverse-phase preparative HPLC using a linear gradient of acetonitrile (5−100%) in water with 0.1% TFA to afford TFA salts of SF-Azo **03** (8.7 mg, 9.1 μmol, 45.8% yield) as a red solid; HRMS (ESI) *m*/*z* calcd for $C_{35}H_{39}N_8O_3$ $[M + H]^+$: 619.3140, found: 619.3142.

*4.4.15. Compound SF-Azo **04**.* **S11** (15 mg, 26 μmol), methyl 3-(piperazin-1-yl)propanoate (31.4 mg, 78.4 μmol), and cesium carbonate (42.6 mg, 131 μmol) were dissolved in acetonitrile (300 μL). The mixture was stirred at 90 °C for 1 h. The resulting residue was washed with saturated $NaHCO_3$ aqueous solution, extracted with ethyl acetate, dried over anhydrous Na_2SO_4, and concentrated. The crude product was purified by flash column chromatography (silica gel, CH_2Cl_2/CH_3OH = 40:1) to afford **S11′** (4.1 mg, 6.3 μmol, 24% yield) as a red solid; ^1H NMR (400 MHz, $CDCl_3$) δ 8.58 (d, *J* = 7.0 Hz, 1H), 8.47 (s, 1H), 7.99 (d, *J* = 8.6 Hz, 2H), 7.92 (d, *J* = 9.0 Hz, 2H), 7.66 (d, *J* = 8.6 Hz, 2H), 7.32 (dd, *J* = 7.4, 1.2 Hz, 1H), 6.79 (d, *J* = 9.4 Hz, 2H), 4.57 (s, 2H), 3.57−3.78 (m, 5H), 3.11 (s, 6H), 2.65−2.77 (m, 2H), 2.63 (s, 3H), 2.36−2.60 (m, 12H), 1.84−2.00 (m, 2H); LRMS (ESI) *m*/*z* calcd for $C_{37}H_{44}N_7O_4$ $[M + H]^+$: 650.34, found: 650.35. **S11′** (4.1 mg, 6.3 μmol) and lithium hydroxide monohydrate (0.8 mg, 20 μmol) were dissolved in 200 μL of THF/H_2O/CH_3OH = 2:1:1 (v/v/v) mixture. The reaction mixture was stirred at room temperature for 0.5 h. The crude product was directly purified by reverse-phase preparative HPLC using a linear gradient of acetonitrile (5−100%) in water with 1% TFA to afford TFA salts of SF-Azo **04** (4 mg, 5 μmol, 70% yield) as a black solid; HRMS (ESI) *m*/*z* calcd for $C_{36}H_{42}N_7O_4$ $[M + H]^+$: 636.3293, found: 636.3295.

4.5. Photophysical Properties Evaluation for SF-Azo 01−04. *4.5.1. Photophysical Property Changes upon Reaction with Hydrazine.* To a solution of SF-Azos (5 μM) in CH_3OH/H_2O (0.5 mL, v/v = 1:1), hydrazine monohydrate (200 mM) in CH_3OH/H_2O (v/v = 1:1) (5 μL) was added. After 1.5 h incubation at 50 °C, 200 μL of reaction mixture was added in a 96-well microplate. Absorption was measured with a clear microplate, and emission was measured with a 96-well black well/clear bottom plate.

4.5.2. Fluorescence Responses Depending on Hydrazine Concentration. To a solution of SF-Azo (5 μM) in CH_3OH/H_2O (0.5 mL, v/v = 1:1), hydrazine monohydrate solution (500, 400, 300, 200, 100, 50, 25, and 5 mM) in CH_3OH/H_2O (0.5 mL, v/v = 1:1) was added. After incubation at 50 °C (1 h for SF-Azo **01**, 2 h for SF-Azo **02** and SF-Azo **03**, and 2.5 h for SF-Azo **04**), reaction mixture (200 μL) was loaded in a 96-well black well/clear bottom plate, and photophysical property changes were measured with a microplate reader. Each compound was excited at the corresponding absorption maxima. The linearity graphs between hydrazine concentration and fluorescent intensity were plotted using GraphPad Prism 5.

4.5.3. Time-Dependent Fluorescence Change. To a solution of 5 μM SF-Azo in CH_3OH/H_2O (v/v = 1:1) mixture at 50 °C, hydrazine monohydrate (2 μL) was added to prepare 200 mM hydrazine solution. Emission spectra of SF-Azo compounds were measured using microplate reader every 3 min until fluorescence signal reached at the maximum intensity. Each SF-Azo was excited at the corresponding absorption maxima. Data were processed with GraphPad Prism 5.

4.5.4. Molar Absorptivity Measurements. To measure the molar absorptivity (ε), a solution of SF-Azo (5, 2.5 and 1 μM) in CH_3OH/H_2O (v/v = 1:1) was prepared. The solution was placed in a quartz cuvette, and the absorbance was measured using a spectrophotometer. To these solutions, hydrazine monohydrate was added to prepare SF-Azo solution with 200 mM hydrazine. The mixtures were incubated at 50 °C for 30 min, and the absorbance was measured by a spectrophotometer. Absorption of SF-Azo probes and their corresponding reduced forms were measured at absorption maximum wavelength (508 nm for SF-Azo **01**, 522 nm for SF-Azo **02**, 492 nm for SF-Azo **03**, 478 nm for SF-Azo **04**, 350 nm for reduced-SF-Azo **01**, 370 nm for reduced-SF-Azo **02**, 360 nm for reduced-SF-Azo **03**, and 410 nm for reduced-SF-Azo **04**). Molar absorptivity values were calculated by GraphPad Prism 5 software, using linear regression.

4.5.5. Selectivity Assay. To solutions of SF-Azo (5 μL) in CH_3OH/H_2O (v/v = 1:1), various compounds (KBr, KI, KCl, KPO_4, KCN, KNO_3, KOH, hydrogen peroxide, cyclohexylethylamine, ethylhexylamine, dimethylamine, ethylenediamine, urea, 200 mM) or hydrazine monohydrate (200 mM) were added. After 30 min incubation at 50 °C, reaction mixtures (200 μL) were loaded in 96-well black well/clear bottom plate and fluorescence was measured using a microplate reader.

4.5.6. Filter Paper Array for Hydrazine Recognition. A corresponding 1 μL stock solution of SF-Azo (1 mM) in CH_3OH was dropped on a 10 cm^2 filter paper, and the paper was dried to prepare a 2 × 2 array (from the upper left corner, clockwise, SF-Azo **01**, **02**, **04**, and **03**). A corresponding 40 μL of hydrazine aqueous solution (1, 0.2, 0.1, 0.05, 0.01, 0.005, and 0.001 M) was dropped on the filter paper arrays with a micropipette. After 30 min incubation of paper array at a 75 °C hot oven, fluorescence was recorded 130 mm above the array using a camera in Samsung smartphone S8 plus with constant optical settings (aperture of F1.7, ISO 800, 4.20 mm focal length with 1/10 s exposure time) under a 365 nm handheld UV lamp. Intensities of the fluorescent spots on the filter paper array were measured using ImageJ software. The areas of the spots were selected to be in oval shape, and the intensities were quantified using the mean gray value measurement. Quantified values were plotted using GraghPad Prism 5.

DOI: 10.1021/acsomega.9b01487
ACS Omega 2019, 4, 14875−14885

■ ASSOCIATED CONTENT

Supporting Information

The Supporting Information is available free of charge on the ACS Publications website at DOI: 10.1021/acsomega.9b01487.

Synthetic procedure and characterization of methyl 3-(piperazin-1-yl)propanoate; reaction condition optimization for intramolecular 1,3-dipolar cycloaddition; cLog *P* values for **S3**−**S5**, **S7**, and SF-Azo **01**−**04**; molar absorptivities (ε) and HPLC analysis of SF-Azo **01**−**04**; LC−MS data of hydrazine-treated SF-Azo **01**; and NMR and HRMS spectra of synthetic compounds (PDF)

■ AUTHOR INFORMATION

Corresponding Authors

*E-mail: sbpark@snu.ac.kr (S.B.P.).
*E-mail: ehkim01@ajou.ac.kr (E.K.).

ORCID

Seung Bum Park: 0000-0003-1753-1433
Eunha Kim: 0000-0002-0766-696X

Present Address

[‖]Department of Chemistry and Biochemistry, University of California, San Diego, La Jolla, California 92093, United States (Y.L.).

Author Contributions

[⊥]M.C.S. and Y.L. contributed equally to this work.

Notes

The authors declare no competing financial interest.

■ ACKNOWLEDGMENTS

This work was supported by Basic Research Program (NRF-2019R1F1A1059121), Priority Research Centers program (2019R1A6A1A11051471), Creative Materials Discovery Program (2019M3D1A1078938), Creative Research Initiative Grant (2014R1A3A2030423), and the Bio & Medical Technology Development Program (2012M3A9C4048780) through the National Research Foundation of Korea (NRF) funded by the Korean Government (Ministry of Science and ICT). Y.L. and M.C.S. were grateful for the fellowship by BK21 Plus Program. The authors thank Yoon Soo Hwang (Seoul National University) for his support in mass analysis and helpful discussion.

■ REFERENCES

(1) Dilworth, J. R. The coordination chemistry of substituted hydrazines. *Coord. Chem. Rev.* **1976**, *21*, 29−62.
(2) Ragnarsson, U. Synthetic methodology for alkyl substituted hydrazines. *Chem. Soc. Rev.* **2001**, *30*, 205−213.
(3) Yamada, K.; Yasuda, K.; Fujiwara, N.; Siroma, Z.; Tanaka, H.; Miyazaki, Y.; Kobayashi, T. Potential application of anion-exchange membrane for hydrazine fuel cell electrolyte. *Electrochem. Commun.* **2003**, *5*, 892−896.
(4) Rothgery, E. F. Hydrazine and Its Derivatives. *Kirk-Othmer Encyclopedia of Chemical Technology*; Wiley, 2004; pp 562−602.
(5) *Hydrazine/Hydrazine Sulfate*; National Center for Environmental Assessment, U.S. Environmental Protection Agency, 1999.
(6) Garrod, S.; Bollard, M. E.; Nicholls, A. W.; Connor, S. C.; Connelly, J.; Nicholson, J. K.; Holmes, E. Integrated Metabonomic Analysis of the Multiorgan Effects of Hydrazine Toxicity in the Rat. *Chem. Res. Toxicol.* **2005**, *18*, 115−122.
(7) Karimi, M. A. Simultaneous Kinetic Spectrophotometric Determination of Hydrazine and Isoniazid Using H-Point Standard Addition Method and Partial Least Squares Regression in Micellar Media. *Croat. Chem. Acta* **2009**, *82*, 729−738.
(8) Budkuley, J. S. Determination of Hydrazine and Sulphite in the Presence of one Another. *Mikrochim. Acta* **1992**, *108*, 103−105.
(9) He, Z. K.; Fuhrmann, B.; Spohn, U. Coulometric microflow titrations with chemiluminescent and amperometric equivalence point detection Bromimetric titration of low concentrations of hydrazine and ammonium. *Anal. Chim. Acta* **2000**, *409*, 83−91.
(10) Yang, Z.; Zheng, X.; Zheng, J. Facile synthesis of three-dimensional porous Au@Pt core-shell nanoflowers supported on graphene oxide for highly sensitive and selective detection of hydrazine. *Chem. Eng. J.* **2017**, *327*, 431−440.
(11) Gao, F.; Wang, Q.; Gao, N.; Yang, Y.; Cai, F.; Yamane, M.; Gao, F.; Tanaka, H. Hydroxyapatite/chemically reduced graphene oxide composite: Environment-friendly synthesis and high-performance electrochemical sensing for hydrazine. *Biosens. Bioelectron.* **2017**, *97*, 238−245.
(12) Smolenkov, A. D.; Shpigun, O. A. Direct liquid chromatographic determination of hydrazines: A review. *Talanta* **2012**, *102*, 93−100.
(13) Oh, J. A.; Shin, H. S. Simple and sensitive determination of hydrazine in drinking water by ultra-high-performance liquid chromatography-tandem mass spectrometry after derivatization with naphthalene-2,3-dialdehyde. *J. Chromatogr. A* **2015**, *1395*, 73−78.
(14) Lichtman, J. W.; Conchello, J. A. Fluorescence microscopy. *Nat. Methods* **2005**, *2*, 910−919.
(15) Meher, N.; Panda, S.; Kumar, S.; Iyer, P. K. Aldehyde group driven aggregation-induced enhanced emission in naphthalimides and its application for ultradetection of hydrazine on multiple platforms. *Chem. Sci.* **2018**, *9*, 3978−3985.
(16) Shi, B.; He, Y.; Zhang, P.; Wang, Y.; Yu, M.; Zhang, H.; Wei, L.; Li, Z. Turn on fluorescent detection of hydrazine with a 1,8-naphthalimde derivative. *Dyes Pigm.* **2017**, *147*, 152−159.
(17) Zhang, R.; Zhang, C.-J.; Song, Z.; Liang, J.; Kwok, R. T. K.; Tang, B. Z.; Liu, B. AIEgens for real-time naked-eye sensing of hydrazine in solution and on a paper substrate: structure-dependent signal output and selectivity. *J. Mater. Chem. C* **2016**, *4*, 2834−2842.
(18) Ban, Y.; Wang, R.; Li, Y.; An, Z.; Yu, M.; Fang, C.; Wei, L.; Li, Z. Mitochondria-targeted ratiometric fluorescent detection of hydrazine with a fast response time. *New J. Chem.* **2018**, *42*, 2030−2035.
(19) Zhang, Y.; Huang, Y.; Yue, Y.; Chao, J.; Huo, F.; Yin, C. A compact fluorescent probe based on o-phthalaldehyde for ultrasensitive detection of hydrazine in gas and solution phases. *Sens. Actuators, B* **2018**, *273*, 944−950.
(20) An, Z.; Li, Z.; He, Y.; Shi, B.; Wei, L.; Yu, M. Ratiometric luminescence detection of hydrazine with a carbon dots−hemicyanine nanohybrid system. *RSC Adv.* **2017**, *7*, 10875−10880.
(21) Lu, Z.; Shi, X.; Ma, Y.; Fan, W.; Lu, Y.; Wang, Z.; Fan, C. A simple two-output near-infrared fluorescent probe for hydrazine detection in living cells and mice. *Sens. Actuators, B* **2018**, *258*, 42−49.
(22) Maji, R.; Mahapatra, A. K.; Maiti, K.; Mondal, S.; Ali, S. S.; Sahoo, P.; Mandal, S.; Uddin, M. R.; Goswami, S.; Quah, C. K.; Fun, H.-K. A highly sensitive fluorescent probe for detection of hydrazine in gas and solution phases based on the Gabriel mechanism and its bioimaging. *RSC Adv.* **2016**, *6*, 70855−70862.
(23) Li, Z.; Zhang, W.; Liu, C.; Yu, M.; Zhang, H.; Guo, L.; Wei, L. A colorimetric and ratiometric fluorescent probe for hydrazine and its application in living cells with low dark toxicity. *Sens. Actuators, B* **2017**, *241*, 665−671.
(24) Li, Z.; Askim, J. R.; Suslick, K. S. The Optoelectronic Nose: Colorimetric and Fluorometric Sensor Arrays. *Chem. Rev.* **2019**, *119*, 231−292.
(25) Jarangdet, T.; Pratumyot, K.; Srikittiwanna, K.; Dungchai, W.; Mingvanish, W.; Techakriengkrai, I.; Sukwattanasinitt, M.; Niamnont, N. A fluorometric paper-based sensor array for the discrimination of

DOI: 10.1021/acsomega.9b01487
ACS Omega 2019, 4, 14875−14885

volatile organic compounds (VOCs) with novel salicylidene derivatives. *Dyes Pigm.* **2018**, *159*, 378−383.
(26) Xu, W.; Liu, W.; Zhou, T.; Yang, Y.; Li, W. A novel PBT-based fluorescent probe for hydrazine detection and its application in living cells. *J. Photochem. Photobiol., A* **2018**, *356*, 610−616.
(27) Hu, C.; Sun, W.; Cao, J.; Gao, P.; Wang, J.; Fan, J.; Song, F.; Sun, S.; Peng, X. A Ratiometric Near-Infrared Fluorescent Probe for hydrazine and Its *in Vivo* Applications. *Org. Lett.* **2013**, *15*, 4022−4025.
(28) Fan, J.; Sun, W.; Hu, M.; Cao, J.; Cheng, G.; Dong, H.; Song, K.; Liu, Y.; Sun, S.; Peng, X. An ICT-based ratiometric probe for hydrazine and its application in live cells. *Chem. Commun.* **2012**, *48*, 8117−8119.
(29) Kim, E.; Lee, Y.; Lee, S.; Park, S. B. Discovery, understanding, and bioapplication of organic fluorophore: a case study with an indolizine-based novel fluorophore, Seoul-Fluor. *Acc. Chem. Res.* **2015**, *48*, 538−547.
(30) Choi, M. G.; Moon, J. O.; Bae, J.; Lee, J. W.; Chang, S. K. Dual signaling of hydrazine by selective deprotection of dichlorofluorescein and resorufin acetates. *Org. Biomol. Chem.* **2013**, *11*, 2961−2965.
(31) Liu, B.; Liu, Q.; Shah, M.; Wang, J.; Zhang, G.; Pang, Y. Fluorescence monitor of hydrazine *in vivo* by selective deprotection of flavonoid. *Sens. Actuators, B* **2014**, *202*, 194−200.
(32) Zhang, J.; Ning, L.; Liu, J.; Wang, J.; Yu, B.; Liu, X.; Yao, X.; Zhang, Z.; Zhang, H. Naked-eye and near-infrared fluorescence probe for hydrazine and its applications in in vitro and in vivo bioimaging. *Anal. Chem.* **2015**, *87*, 9101−9107.
(33) Ma, J.; Fan, J.; Li, H.; Yao, Q.; Xia, J.; Wang, J.; Peng, X. Probing hydrazine with a near-infrared fluorescent chemodosimeter. *Dyes Pigm.* **2017**, *138*, 39−46.
(34) Sun, M.; Guo, J.; Yang, Q.; Xiao, N.; Li, Y. A new fluorescent and colorimetric sensor for hydrazine and its application in biological systems. *J. Mater. Chem. B* **2014**, *2*, 1846−1851.
(35) Reja, S. I.; Gupta, N.; Bhalla, V.; Kaur, D.; Arora, S.; Kumar, M. A charge transfer based ratiometric fluorescent probe for detection of hydrazine in aqueous medium and living cells. *Sens. Actuators, B* **2016**, *222*, 923−929.
(36) Tiensomjitr, K.; Noorat, R.; Wechakorn, K.; Prabpai, S.; Suksen, K.; Kanjanasirirat, P.; Pewkliang, Y.; Borwornpinyo, S.; Kongsaeree, P. A rhodol-based fluorescent chemosensor for hydrazine and its application in live cell bioimaging. *Spectrochim. Acta, Part A* **2017**, *185*, 228−233.
(37) Leung, C.-H.; Daniel, S.-H. C.; Man, B. Y.-W.; Wang, C.-J.; Lam, W.; Cheng, Y.-C.; Fong, W.-F.; Hsiao, W.-L. W.; Ma, D.-L. Simple and Convenient G-Quadruplex-Based Turn-On Fluorescence Assay for 3′ → 5′ Exonuclease Activity. *Anal. Chem.* **2011**, *83*, 463−466.
(38) Zhang, C.-R.; Wang, Y.-L. A Simple and Efficient Method for the Reduction of Azo Compounds. *Synth. Commun.* **2003**, *33*, 4205−4208.
(39) Koppes, W. M.; Moran, J. S.; Oxley, J. C.; Smith, J. L. Azo bond hydrogenation with hydrazine, R−NHNH$_2$, and hydrazobenzene. *Tetrahedron. Lett.* **2008**, *49*, 3234−3237.
(40) Rollas, S. Reduction of aromatic and heteroaromatic azo compounds with hydrazine hydrate. *Marmara Pharm. J.* **2010**, *1*, 41−46.
(41) Chevalier, A.; Massif, C.; Renard, P. Y.; Romieu, A. Bioconjugatable azo-based dark-quencher dyes: synthesis and application to protease-activatable far-red fluorescent probes. *Chem. − Eur. J.* **2013**, *19*, 1686−1699.
(42) Chevalier, A.; Hardouin, J.; Renard, P. Y.; Romieu, A. Universal Dark Quencher Based on "Clicked" Spectrally Distinct Azo Dyes. *Org. Lett.* **2013**, *15*, 6082−6085.
(43) Zhou, D.; Wang, Y.; Jia, J.; Yu, W.; Qu, B.; Li, X.; Sun, X. H-Bonding and charging mediated aggregation and emission for fluorescence turn-on detection of hydrazine hydrate. *Chem. Commun.* **2015**, *51*, 10656−10659.
(44) Cheng, X.; Zhang, R.; Cai, X.; Liu, B. A reusable and naked-eye molecular probe with aggregation-induced emission (AIE) characteristics for hydrazine detection. *J. Mater. Chem. B* **2017**, *5*, 3565−3571.
(45) Kim, E.; Koh, M.; Lim, B. J.; Park, S. B. Emission wavelength prediction of a full-color-tunable fluorescent core skeleton, 9-aryl-1,2-dihydropyrrolo[3,4-b]indolizin-3-one. *J. Am. Chem. Soc.* **2011**, *133*, 6642−6649.
(46) Piao, W.; Tsuda, S.; Tanaka, Y.; Maeda, S.; Liu, F.; Takahashi, S.; Kushida, Y.; Komatsu, T.; Ueno, T.; Terai, T.; Nakazawa, T.; Uchiyama, M.; Morokuma, K.; Nagano, T.; Hanaoka, K. Development of azo-based fluorescent probes to detect different levels of hypoxia. *Angew. Chem., Int. Ed.* **2013**, *52*, 13028−13032.
(47) Shin, N.; Hanaoka, K.; Piao, W.; Miyakawa, T.; Fujisawa, T.; Takeuchi, S.; Takahashi, S.; Komatsu, T.; Ueno, T.; Terai, T.; Tahara, T.; Tanokura, M.; Nagano, T.; Urano, Y. Development of an Azoreductase-based Reporter System with Synthetic Fluorogenic Substrates. *ACS Chem. Biol.* **2017**, *12*, 558−563.
(48) Lee, Y.; Cho, W.; Sung, J.; Kim, E.; Park, S. B. Monochromophoric Design Strategy for Tetrazine-Based Colorful Bioorthogonal Probes with a Single Fluorescent Core Skeleton. *J. Am. Chem. Soc.* **2018**, *140*, 974−983.
(49) Al Zoubi, W.; Kamil, M. P.; Yang, H. W.; Ko, Y. G. Electron-Donor and -Acceptor Agents Responsible for Surface Modification Optimizing Electrochemical Performance. *ACS Appl. Mater. Interfaces* **2017**, *9*, 28967−28979.
(50) Choi, E. J.; Kim, E.; Lee, Y.; Jo, A.; Park, S. B. Rational perturbation of the fluorescence quantum yield in emission-tunable and predictable fluorophores (Seoul-Fluors) by a facile synthetic method involving C-H activation. *Angew. Chem., Int. Ed.* **2014**, *53*, 1346−1350.
(51) Cavaiuolo, M.; Paramithiotis, S.; Drosinos, E. H.; Ferrante, A. Development and optimization of an ELISA based method to detect Listeria monocytogenes and Escherichia coli O157 in fresh vegetables. *Anal. Methods* **2013**, *5*, 4622−4627.
(52) Masdor, N. A. Determination of the Detection Limit using the Four-Parameter Logistic Model for The Double-Antibody Sandwich ELISA for the Rapid Detection of *Bacillus cereus* in Food. *JEMAT* **2017**, *5*, 12−13.
(53) Ross, W. C. J.; Warwick, G. P. Reduction of Cytotoxic Azo Compounds by Hydrazine And by the Xanthine Oxidase-Xanthine System. *Nature* **1955**, *176*, 298−299.
(54) Mutlu, H.; Geiselhart, C. M.; Barner-Kowollik, C. Untapped potential for debonding on demand: the wonderful world of azo-compounds. *Mater. Horiz.* **2018**, *5*, 162−183.
(55) Peor, N.; Sfez, R.; Yitzchaik, S. Variable Density Effect of Self-Assembled Polarizable monolayers on the Electronic Properties of Silicon. *J. Am. Chem. Soc.* **2008**, *130*, 4158−4165.
(56) Saccone, M.; Dichiarante, V.; Forni, A.; Goulet-Hanssens, A.; Cavallo, G.; Vapaavuori, J.; Terraneo, G.; Barrett, C. J.; Resnati, G.; Metrangolo, P.; Priimagi, A. Supramolecular hierarchy among halogen and hydrogen bond donors in light-induced surface patterning. *J. Mater. Chem. C* **2015**, *3*, 759−768.

DOI: 10.1021/acsomega.9b01487
ACS Omega 2019, 4, 14875−14885